Differential Growth Rates, Rather Than Compaction, Determine Left Ventricular Wall Formation

Jaeike Faber
Department of Medical Biology, Amsterdam Cardiovascular Sciences, Amsterdam University Medical Centres, Amsterdam, The Netherlands

Rob Wüst
Laboratory for Myology, Faculty of Behavioural and Movement Sciences, Amsterdam Movement Sciences, Vrije Universiteit Amsterdam, Amsterdam, The Netherlands

Inge Dierx
Department of Medical Biology, Amsterdam Cardiovascular Sciences, Amsterdam University Medical Centres, Amsterdam, The Netherlands

Janneke Hummelink
Department of Medical Biology, Amsterdam Cardiovascular Sciences, Amsterdam University Medical Centres, Amsterdam, The Netherlands

Diederik Kuster
Department of Physiology, Amsterdam Cardiovascular Sciences, Amsterdam University Medical Centres, Amsterdam, The Netherlands

Edgar Nollet
Department of Physiology, Amsterdam Cardiovascular Sciences, Amsterdam University Medical Centres, Amsterdam, The Netherlands

Antoon Moorman
Department of Medical Biology, Amsterdam Cardiovascular Sciences, Amsterdam University Medical Centres, Amsterdam, The Netherlands

Damián Sánchez-Quintana
Department of Anatomy and Cell Biology, Universidad de Extremadura, Badajoz

Allard van der Wal
Department of Pathology, Amsterdam University Medical Centres, Amsterdam, The Netherlands

Vincent Christoffels
Department of Medical Biology, Amsterdam Cardiovascular Sciences, Amsterdam University Medical Centres, Amsterdam, The Netherlands

Bjarke Jensen (b.jensen@amsterdamumc.nl)
Department of Medical Biology, Amsterdam Cardiovascular Sciences, Amsterdam University Medical Centres, Amsterdam, The Netherlands

Research Article

Keywords: Allometric growth, compaction, Left Ventricular Non-Compaction, heart development, embryology

Posted Date: June 24th, 2021

DOI: https://doi.org/10.21203/rs.3.rs-608669/v1

Abstract

Trabecular muscle makes up most of the ventricular wall of the human embryo. It is presumed that compaction in the foetal period changes ventricular wall morphology by converting weaker trabeculae to stronger compact muscle. Using developmental series covering the embryonic and foetal periods of human, mouse and chicken, we show ventricular morphology is determined by differential rates of positive growth of trabecular and compact layers rather than compaction. In mouse, foetal cardiomyocytes are relative weak, but adult trabecular and compact cardiomyocytes are equally strong. In foetal and adult humans, trabecular and compact myocardium exhibit a similar abundance of immunohistochemically detected vascular, mitochondrial and sarcomeric proteins. Even in human noncompaction, a congenital malformation characterized by excessive trabeculation, the trabecular and compact muscle are similar. In conclusion, trabecular and compact myocardium are equally equipped for force production and their proportions are determined not by compaction, but by differential growth rates.

Introduction

The relative thickness of the trabeculated over the compact myocardial layer in the normal adult left ventricle varies according to a log-normal distribution [1,2] whereby a ratio of > 2.3 [3] is thought to be the most sensitive diagnostic criterion for Left Ventricular Non-Compaction (LVNC) cardiomyopathy [4]. This cardiomyopathy is characterised by prominent left ventricular trabeculae and, concomitantly, deep inter-trabecular recesses. LVNC has been associated with ventricular dilatation, systolic dysfunction, arrhythmias and embolic events [5,6]. The notion that trabecular myocardium is ill-equipped to maintain good pump function has, therefore, been implied [7]. However, from large cohort studies a relationship between a hypertrabeculated left ventricle and cardiac dysfunction has not come forward [8,9]. The function of the trabecular myocardium has never been investigated directly, also because trabecular myocardium is difficult to model due to its complex 3 dimensional structure [10].

Like the name implies, LVNC is thought to result from a failure of compaction [11]. Compaction has been described as a process of compression of trabecular myocardium to form part of the compact wall [12], thereby simultaneously decreasing the amount of trabecular myocardium and increasing the amount of compact myocardium [13]. It has been claimed to occur in the embryonic period (e.g. [14,15]), the foetal period (e.g. [16,17]), or even up to birth [18]. Nevertheless, there are no comprehensive quantitative assessments of compact and trabecular layer growth to support the notion of compaction [19]. In fact, only two studies have quantified the trabecular layer volume in embryonic development and both report a continuous increase and not a decrease as would be expected if compaction was to occur (see [19]).

Our aim was to investigate left ventricular free wall development during gestation in order to measure the magnitude and timing of compaction. Because the LVNC diagnosis depends on ratio in layer thickness [3,20] and calculated ventricular volume as proxy for myocardial mass [21], those were also investigated. We compared the findings from human to the growth curves we established for mouse and chicken, which

are the most-used animal models in cardiac development with compact ventricular walls. Finally, we investigated if there are functional differences between trabecular and compact myocardium.

Methods

All studies were in compliance with the Helsinki Declaration and all protocols were approved by the Medical Ethics Committee of the University of Amsterdam, The Netherlands. The study was carried out in compliance with the ARRIVE guidelines and animal care and experiments conformed to the Directive 2010/63/EU of the European Parliament. All animal work was approved by the Animal Experimental Committee of the Amsterdam University Medical Centers, location AMC, Amsterdam, and was carried out in compliance with the Dutch government guidelines, approved by the Central Committee Animal Experiments.

Hearts

Human

Single sections from transversely sectioned hearts from 3 to 36 weeks of gestation were used for morphometric analysis (N = 37). The origins of twenty hearts were previously described [22,23]. Eight sections were derived from the Medical Biology Department archives at Amsterdam UMC. These sections had all been immunofluorescently stained for cardiac troponin I [22] or histochemically with haematoxylin and eosin. Nine foetal sections, stained with Masson Trichrome, were provided by Dr. Sánchez-Quintana, and these hearts were obtained with permission of the Bioethical Committee on Human Research of the University of Extremadura, Spain.

Paraffin sections of previously described aborted foetal hearts with either normal (N = 2) or LVNC morphology (N = 4) [24], and sections from adult autopsy derived morphologically normal human hearts (N = 6) were obtained from archives of the Pathology Department of Amsterdam UMC, and used for the functional phenotypical analysis of myocardium. Informed consent was obtained for all autopsies from the decedent's next of kin and for the anonymous use of archived autopsy materials a waiver was granted by the Medical Ethics Committee of the University of Amsterdam.

Mouse

FVB/NRj wild-type mouse embryos (*Mus musculus*, Janvier labs, www.janvier-labs.com) of 9.5 to 17.5 gestational days were obtained from a variety of in-house bred litters. Hearts from these mice, and from postnatal mice from day 0 to 23 were isolated and fixed with 4% paraformaldehyde in phosphate buffered saline for morphometric analysis (N = 47).

For the mitochondrial activity assay, samples of left ventricular papillary muscle with surrounding trabeculae carneae, compact wall, as well as left atria were collected from freshly killed adult surplus mice (N = 6).

For the contractile force analysis, whole ventricles from foetal mice at 15.5 gestational days (N = 2), as well as separated left ventricular compact and trabecular myocardium from surplus wild-type adult hearts (N = 6) were obtained by fine dissection before being snap frozen in liquid nitrogen.

Chicken

Wild-type chicken embryos (*Gallus gallus*, Drost BV, Nieuw Loosdrecht, The Netherlands) of 2 to 19 gestational days were obtained from eggs incubated in a humidified rocking stove at 38.5°C (N = 28). Whole embryos or isolated hearts were fixed with 4% paraformaldehyde in phosphate buffered saline. Additionally, sections of Bouin fixed chicken embryos, previously histochemically stained for troponin bound antibodies (N = 10) or haematoxylin and eosin (N = 6), were included from the Medical Biology Department archives at Amsterdam UMC.

Morphometry

In situ hybridisation

After fixation, tissues were embedded in paraffin (Paraplast, Leica) and sectioned at 10 µm thickness with a Leica microtome. Sections at approximately 4 chamber view were then stained with digoxigenin labelled RNA probes against *TNNI3* for mouse (1 ng/µl) and chicken (0.1 ng/µl) as previously described [25].

Morphometric assessments

On images of stained hearts, a wheel with spokes at 30° intervals was projected (Online Fig. 1A). The centre of the wheel was placed at the centre of the left ventricular lumen while the spoke of 0° was placed approximately at the atrioventricular canal, the spoke of 180° was located towards the apex of the heart and the spoke of 330° pointed towards the aorta. The thickness of the lumen, the trabeculated myocardial layer, and compact myocardial layer were measured along the spokes of 0° to 210° with ImageJ 1.51j8 software (National Institutes of Health, USA) (Online Fig. 1B). The border between the myocardial layers was determined on sight by following the free lumen to where the crevasses between the trabeculae were deepest.

The surface areas of the compact and trabeculated myocardium between each spoke from 0° to 210° were measured on binary transformed images (Online Fig. 1C) with the polygon selection tool in ImageJ after the free lumen area had been subtracted by projection of an, as large as possible, ellipse in the ventricular cavity that did not cross any myocardial structures. Both the total surface area and the percentage of myocardialised surface area were collected (Online Fig. 1D). In case a spoke did not cross any left ventricular myocardium, for example if the 0° spoke lay in the atrioventricular canal, or when parts of the section were damaged, measurements were resumed at the next suitable spoke. In case no clear distinction between blood and myocardium could be made in the histochemically stained sections, no surface area measurements were taken.

To calculate the and the the following equations were used:

$$(1)\ V_{compact} = \widetilde{\frac{4}{3}\pi r^3} \times \frac{A_{compact} \times \frac{\%\widetilde{Myocardium}_{compact}}{100}}{A_{total}}$$

$$(2)\ V_{trabecular} = \widetilde{\frac{4}{3}\pi r^3} \times \frac{A_{trabecular-lumen} \times \frac{\%\widetilde{Myocardium}_{trabecular-lumen}}{100}}{A_{total}}$$

The tilde stands for median, so the median of each total ventricular volume, $V_{total} = \frac{4}{3}\pi r^3$, with each measured total spoke length taken as *r*, was multiplied with the median of each myocardial fraction of surface area. Because the measured surface areas are not fully myocardial but also contain intertrabecular lumen and coronary artery lumina, the surface areas were corrected for the myocardial occupancy: %Myocardium. For the trabecular fraction, the lumen area, as obtained by placement of the ellipse, had been subtracted.

Functional phenotypical analysis

Histochemical staining

Sections (5µm) of formalin fixed paraffin embedded blocks of transmural human adult left ventricular wall were stained with Picrosirius red, with which collagen stains red and muscle orange (the stain was differentiated for 2 min in 0.01 M HCl). Sections were filtered for all colours except red in ImageJ and then converted to binary images. The staining intensity for trabecular and compact layer was then quantified as the grey scale value of the area trabecular and compact area respectively.

Immunofluorescencence and immunohistochemistry

For functional phenotypical analysis, sections of human foetal and adult left ventricles were rehydrated as described for in situ hybridisation. After rinsing, the samples were cooked in unmasking solution (citrate based Antigen Unmasking Solution, Vector, H3300, Lt. ZB1016). Samples were either incubated with Triton 0.5% and then TNT or immediately in TNT if a membrane antibody was used. Hereafter, samples were blocked with TNB (0.1M Tris-HCl, pH 7.5; 0.15M NaCl; 0.5% blocking powder (TSA Enhancement kit, Perkin & Elmer NEL702A)) for at least 30 minutes. Sections were then incubated with primary antibodies against complex 4 of the mitochondrial respiratory chain COX4 (1:200, monoclonal mouse-anti-human, Abcam, 20E8C12), and cardiac troponin I cTnI (1:200, polyclonal goat-anti-human, HyTest, 4T21/2) at room temperature overnight. The next day the sections were rinsed in TNT and incubated in the dark with secondary antibodies Donkey-anti-rabbit Alexa 555 (1:250, 2mg/ml 09-08-18, Invitrogen A31572, Lt. 1945911) and 1µl Donkey-anti-mouse Alexa 488 (1:250, 13-10-17, Invitrogen A21202, Lt. 1890861). After 2 hours they were washed again 3x for 5 min in TNT 1x before being mounted with DAPI (1:250) in PBS/glycerol (1:1). For detection of endothelium and mitochondrial-surface protein we used a primary antibody against CD31 (clone JC70A, Dakopatts, Denmark) and MAB1273

respectively (1:100, monoclonal mouse-anti-human, Sigma-Aldrich,), which were visualised with DAB+ (Dako) in an immunoperoxidase stain and faintly counterstained with haematoxylin.

Images of sections were imported to ImageJ and converted to 8 bit (grey scale) images. In the adult samples, staining intensities in the trabecular layer, compact layer and epicardium were calculated respectively as their average grey scale values, which informed us on the relative amount of detected protein in each different tissue area per section. For the foetal specimens, the signal intensity of 5 (epicardium) to 10 (trabecular and compact) areas within a single section were pooled and median corrected per specimen.

Functional analysis

Mitochondrial respiration

From 6 adult mice we isolated left ventricular papillary muscle with surrounding trabeculae carneae, compact wall, and left atrium. The mitochondrial function in these tissues were assessed separately as previously described [26].

Tissue samples were permeabilized with 50 µg/mL saponin for 30 minutes at 4 ºC in a preservation solution consisting of 2.8 mM CaEGTA, 7.2 mM EGTA, 5.8 mM ATP, 6.6 mM $MgCl_2$, 20 mM taurine, 15 mM phosphocreatine, 20 mM imidazole, 0.5 mM dithiothreitol and 50 mM MES buffer (pH 7.1). Tissue was subsequently washed in respiration solution, containing 0.4 mM EGTA, 3 mM $MgCl_2$, 60 mM K-lactobionate, 20 mM taurine, 10 mM KH_2PO_4, 20 mM HEPES, 110 mM sucrose and 1 g/l fatty acid free bovine serum albumin (pH 7.1), quickly blotted dry, weighed and transferred to a respirometer (Oxygraph-2k, Oroboros Instruments, Innsbruck, Austria) in respiration solution at 37°C. Oxygen concentration was maintained above 300 µM throughout the experiment to avoid limitations in oxygen supply. Leak respiration was assessed after addition of 10 mM sodium glutamate, 0.5 mM sodium malate and 5 mM sodium pyruvate. Outer-mitochondrial membrane damage was tested by the addition of 10 µM cytochrome c, but no sampled showed an increase of > 15% in respiration compared to the addition of 2.5 mM ADP. Maximal NADH-linked (via complex I) respiration was assessed after the addition of cytochrome c, that is, after alleviating possible effects of outer-membrane damage. Maximal oxidative phosphorylation capacity (OXPHOS) was measured after addition of 10 mM succinate. Maximal uncoupled respiration was measured after the stepwise addition of 0.01 µM FCCP (carbonylcyanide-4-(trifluoromethoxy)-phenylhydrazone). Respiration values were normalized to wet weight and expressed in pmol $O_2 \cdot s^{-1} \cdot mg^{-1}$.

Force generation

To investigate if trabecular and compact myocardium are functionally different, mouse heart samples were subjected to calcium induced contraction force measurements from which maximal active (F_{max}) and passive force (F_{pas}) as well as the Hill coefficient (nHill), and EC_{50}, were obtained.

Snap-frozen samples were defrosted and ground up in relax solution containing 1 mM Mg^{2+}, KCl 145 mM, 2 mM EGTA, 4 mM ATP, 10 mM imidazole (pH 7.0). After a 5 minute incubation in 0.5% triton X-100 in relax solution, single adult cardiomyocytes or small clusters of foetal cardiomyocytes were selected on the basis of a minimal width of 20µm and a maximal width of 61µm, with visible sarcomeric structures to be measured after a force transducer and a piezoelectric motor needle were glued onto the cell with shellac.

Calcium response curves were measured at a sarcomeric length of 2.2 µm [27]. To this end, glued cells or cell clusters were transferred into a series of solutions with a $[Ca^{2+}]$ of $10^{-4.5}$, $10^{-4.5}$, $10^{-5.4}$, 10^{-6}, $10^{-5.2}$, $10^{-5.8}$, 10^{-5}, $10^{-6.2}$, and $10^{-4.5}$ M respectively. The total force was the combined active (F_{act}) and passive force (F_{pas}) with F_{pas} being the force generated after transferring the tissue back to relax solution and slackening the tissue length by 30%. The maximal force (F_{max}) was the F_{act} obtained during the second subjection to $[Ca^{2+}]$ $10^{-4.5}$ M. All forces were corrected for cell cross-sectional area (*A = width X depth X Π*). The Hill coefficient (nHill), and EC_{50}, were calculated from the established relative calcium response curves in GraphPad prism using a non-linear curve fit for the dose-response curve agonist vs. response – variable slope (four parameters) using 1 and 0 as top and bottom constraints. Only cells with a rundown of < 30% between the second and last $[Ca^{2+}]$ of $10^{-4.5}$ M were taken along for analysis.

Imaging

A Leica CTR5000 light microscope with a DFC450 camera was used to image the histochemical and *in situ* hybridisation stains. Immunofluorescent stains were imaged using a Leica CTR6000 microscope mounted with a Retiga EXi Fast camera (SN:Q19688, Qimaging). Confocal microscopy was performed with a Leica TCS SP8 SMD mounted on a Leica DMI6000 inverted microscope with objective HC PL APO CS2 63x/1.40.

Statistics

Analyses were performed using GraphPad Prism 8.3.0 (GraphPad Software, LLC). Error bars for the thickness slopes represent 95% confidence intervals. In all other figures error bars represent standard deviations and lines represent means. Growth curves were compared with linear regression analyses and correlation of thickness growth with age was calculated with a Pearson correlation coefficient. Staining signal intensities were compared with Tukey corrected One-Way ANOVA or Mixed Effects Analysis. In case of only 2 groups a paired t-test was performed.

Results

Ventricular wall growth

The human heart grows from 0.07 to 4.7 cm in length between 20 days and 36 weeks of gestation. Early embryonic hearts fit *in toto* into individual trabeculae of the late foetal heart (Fig. 1A). The trabecular

layer thickness never decreased as would be expected if compaction took place (Fig. 1B). Dramatic changes to the LVNC-diagnostic ratio, however, did occur in the embryonic period (Fig. 1C). This was due to changes in layer growth rates. From approximately 22–31 gestational days, the trabecular layer increased faster in thickness than the compact layer (16 ± 9 μm/day, F = 21.26, 1 degree of freedom versus 0 ± 1 μm/day, difference $p < 0.001$, F = 0.64, 1 degree of freedom). This caused a thickness ratio increase to 10.2. This is much higher than the clinical LVNC cut-off value of 2.3. From approximately 32 to 56 gestational days, the growth rates of both layers were not significantly different (trabecular myocardium 2 ± 7 μm/day, F = 0.87, 1 degree of freedom, compact myocardium 6 ± 3 μm/day, F = 0.79, 1 degree of freedom, difference $p = 0.309$). However, the trabecular thickness growth rate did not correlate with age ($p = 0.387$), while the compact wall did ($p = 0.003$). This indicates that only the trabecular thickness remained constant, causing the thickness ratio to decrease to below the LVNC threshold. Since the ventricles continuously expand, the compact and trabecular layer volumes have to grow to maintain a stable layer thickness, which is seen most clearly in late embryonic development where the trabecular layer thickness is stable and the volume grows (Fig. 1D), see also Online Fig. 2. In the foetal period, both the trabecular and compact layer grew continuously with no difference in the rate of thickening (trabecular slope 19 ± 8 μm/day, F = 29.84, 1 degree of freedom, compact slope 15 ± 5 μm/day, F = 44.11, 1 degree of freedom, difference $p = 0.327$). This stabilised the thickness ratio below the LVNC threshold.

In mouse, the most used animal model for studying LVNC, and chicken, the animal model in which the process of compaction of the base of the trabeculae was demonstrated for the right ventricle [28], the growth curves of the trabeculated and compact myocardium were similar to human. This was also illustrated by the transient peak in layer thickness ratio in the embryo (Fig. 2). No decrease in absolute trabecular layer thickness was seen (Fig. 2B), even if the trabecular layer was labelled to be excessive in younger stages and exceedingly regressed in older stages (Online Fig. 3). Although the post-natal mouse hearts appeared to show a larger variation in trabecular layer thickness between specimens than foetal human and late-gestational chicken, at no point was there a re-increase in thickness ratio (Fig. 2C) or a decrease in trabecular volume (Fig. 2D).

Since the trabecular and compact growth rate in foetal stages is similar, we hypothesised that, despite the difference in gross morphology, trabecular and compact myocardium may be phenotypically similar.

Trabecular and compact myocardial functional phenotype

To test for similarity in myocardial phenotype, we assessed the relative abundance of proteins related to ATP production (mitochondrial protein), force generation (sarcomeric protein) and blood supply (vascular endothelium) in adult human trabecular and compact myocardium. Since sarcomeric proteins occur in tissues with a fixed stoichiometry [29], values on cardiac troponin I (cTnI) are a good indicator of total sarcomeric protein in a cell. The staining signal was not different between trabecular and compact myocardium ($p = 0.247$, F = 62.24, 2 degrees of freedom), but greater than that of non-myocardial tissue (Fig. 3A). Similarly, there was no difference in the amount of mitochondrial protein COX4 ($p = 0.857$, F = 36.89, 2 degrees of freedom) (Fig. 3A), mitochondrial surface protein MAB1273 ($p = 0.802$, F = 63.56, 2

degrees of freedom) (Fig. 3B), and endothelial protein CD31 ($p = 0.283$, $F = 86.67$, 2 degrees of freedom) (Fig. 3C) based on signal intensity. The distance between capillaries was also similar indicating similar cardiomyocyte size (17.9 ± 1.3 µm in trabecular versus 18.9 ± 2.9 µm in compact myocardium, $p = 0.284$, T value = 1.237, 4 degrees of freedom, N = 5, two-tailed paired Student's T-test) and similar microvascular density. Only collagen was slightly more abundant in the trabecular layer, which, however, contained a few collagenous chordae tendineae ($p = 0.038$, $F = 50.05$, 2 degrees of freedom, Fig. 3D).

Trabecular and compact myocardial function

Despite the absence of differences in myocardial sarcomeric proteins, mitochondrial proteins and capillary densities, we next tested the hypothesis that the trabecular and compact myocardium have similar mitochondrial and contractile function. Myocardial work requires ATP and is therefore correlated with cellular oxygen consumption [30]. Therefore, we compared mitochondrial respiration in trabecular and compact muscle. In adult mouse hearts, the leak respiration was higher in trabecular than in compact myocardium ($p = 0.033$) and the left atrial wall ($p = 0.027$), but the NADH-linked respiration, maximal oxidative phosphorylation capacity and maximal uncoupled respiration did not differ between the two myocardial tissues ($p = 0.999$, $p = 0.989$, $p = 0.997$ respectively), while they did show higher mitochondrial respiration than the left atrial wall (Fig. 4A).

To assess the force generating capacity of trabecular and compact myocardium, we compared force production of isolated cardiomyocytes. There was no difference between adult compact and trabecular cardiomyocytes in maximum force production (F_{max}, $p = 0.959$), average passive force, (F_{pas}, $p = 0.060$), or calcium sensitivity ($p = 0.075$) (Fig. 4B-G). Trabecular myocardium is thought to be more embryonic-like than compact myocardium [31], but both trabecular and compact adult cardiomyocytes had much greater maximum force production than foetal ventricular myocardium ($p < 0.001$ and $p < 0.001$, $F = 19.83$, 2 degrees of freedom) (Fig. 4C-D).

Trabecular and compact myocardium are similar in non-compaction

Because trabecular and compact myocardial function were similar, we speculated that the trabecular and compact myocardium may be equally affected in non-compaction. We found no significant differences between compact and trabecular myocardium regarding the COX4 ($F = 51.64$, 5 degrees of freedom, Fig. 5A), MAB1273 ($F = 280.1$, 5 degrees of freedom, Fig. 5B), and CD31 ($F = 75.77$, 5 degrees of freedom, Fig. 5C) signal intensity in normal ($p = 1.000$, $p = 0.224$, $p = 0.449$) and LVNC cases ($p = 0.574$, $p = 0.375$, $p = 0.990$). Sarcomeric protein cTnI signal intensity was significantly higher in trabecular than in compact myocardium in normal ($p = 0.0003$) and LVNC hearts ($p = 0.001$) ($F = 87.49$, 5 degrees of freedom, Fig. 5D). Even though these data do not provide evidence of altered mitochondrial or sarcomeric protein densities in LVNC, we found no indication that only the trabecular myocardium would be less equipped for contractile function in LVNC.

Discussion

Here, we show for the first time that in the foetal period the left ventricular trabecular and compact myocardium are surprisingly similar in terms of growth, functional phenotype, and function. While this is surprising when premised on hypertrabeculation in LVNC causing heart failure, our findings are fully consistent with the growing number of cohort studies showing no or only very slight correlations between extent of trabeculations and pump function [4,8,9].

Differential growth rate determines left ventricular wall development

Histological techniques showed continuous growth of both trabecular and compact myocardium during development in human, mouse, and chicken. This indicates that differential growth shapes the left ventricular wall. Differential growth also forms other chambers of the heart and, more generally, embryonic organs, limbs, head, etc. [32,33]. We found no evidence for compaction or a loss of myocardium of the trabecular layer, as would be expected when compaction would occur, though we did see dramatic changes to the LVNC-diagnostic criterium of wall ratio in the embryo. So, differential growth can lead morphometrically to LVNC positivity, in the absence of compaction. LVNC is, therefore, likely a misnomer.

Since there may be distinct phases in trabecular layer thickness growth, natural and pathological variation in the duration of these phases may impact on wall ratio. Because the ratio does not indicate which layer behaves abnormally, patients with LVNC may have either excessive trabeculae or an underdeveloped compact wall [34–36]. Also, a longer duration of fast trabecular growth does not necessarily imply inferiority of the trabecular muscle. In fact, in our cases of LVNC, the trabecular and compact layers appeared equally equipped with vasculature, mitochondria and sarcomeric protein.

No functional phenotypical differences between trabecular and compact myocardium

Generating contractile force requires a high metabolic rate which has to be supported by the presence of a vast capillary network and a high mitochondrial density. There was no evidence that this was lacking in adult trabecular myocardium and it has long been demonstrated, for example, that the papillary muscles and trabeculae carneae are as vascularized as the neighbouring compact wall [37,38]. Likely, the initial differences between embryonic trabeculae and embryonic compact myocardium regarding functional phenotype disappear in the older heart as is also supported by the absence of an unambiguous marker for trabecular myocardium in the adult heart [24,39–41].

No functional differences between trabecular and compact myocardium

Our results indicate that adult cardiomyocytes from the trabecular and compact layer are equally equipped for force generation which is supported by in silico genetic and phenotypic correlation assays [42]. The maximal generated forces we described, corresponded to those in other species which have been inferred from systemic blood pressure, wall thickness and ventricular dimensions [43]. Foetal cardiomyocytes were found to be less strong than adult cardiomyocytes, again confirming that adult trabecular myocardium does not have an embryonic identity [24]. That the vast majority of people with

hypertrabeculation, diagnosed as LVNC, are asymptomatic is consistent with the trabecular and compact myocardium having a similar contractile force potential [8,44,45].

Limitations

Because of the morphometric analysis sensitivity it is possible that there is still a small contribution of compaction to the growth of the compact wall. However, our analysis excludes a large contribution, and, therefore, it is unlikely that non-compaction can lead to the extremely trabeculated ventricles observed in some patients with LVNC [20].

Compaction has been previously described for chicken in the right ventricle [28] and has been suggested to occur in the left ventricle [46]. However, we could not replicate the same steep increase in compact wall thickness around day 10 in chick development as reported previously [46] even when artificially shifting our trabecular to compact borderlines (Online Fig. 3).

Conclusions

We assessed left ventricular trabecular and compact layer growth in human, mouse and chicken. The left ventricular wall acquires its adult form by differential growth rather than by compaction (conversion) of trabecular to compact myocardium. LVNC is, therefore, likely a misnomer and its diagnosis on the basis of layer thickness ratio alone is uninformative on the overall ventricular morphology and functional state of myocardium. Because we found no difference in trabecular and compact myocardial functional phenotype and function, it appears that it is not trabecular weakness that causes heart failure in some patients with LVNC.

Abbreviations

F_{max}, maximum force (measured in cardiomyocytes)

F_{pas}, passive force upon stretching (measured in cardiomyocytes)

F_{act}, active force induced by calcium (measured in cardiomyocytes)

nHill, Hill coefficient of sarcomeric calcium sensitivity

LVNC, left ventricular non-compaction cardiomyopathy

Declarations

Acknowledgements

We would like to thank Fernanda Bosada, Rajiv Mohan, Antoinette van Ouwerkerk, Corrie de Gier-de Vries and Maurice van den Hoff for their assistance.

Author contributions

Conceptualization: Jaeike W. Faber, Bjarke Jensen; Methodology: Jaeike W. Faber, Diederik W. D. Kuster, Bjarke Jensen; Formal analysis and investigation: Jaeike W. Faber, Rob C. I. Wüst, Inge Dierx, Janneke A. Hummelink, Edgar Nollet; Writing - original draft preparation: Jaeike W. Faber, Bjarke Jensen; Writing - review and editing: Jaeike W. Faber, Rob C. I. Wüst, Inge Dierx, Janneke A. Hummelink, Diederik W. D. Kuster, Edgar Nollet, Antoon F.M. Moorman, Allard van der Wal, Vincent M. Christoffels, Bjarke Jensen; Funding acquisition: Antoon F. M. Moorman; Resources: Diederik W. D. Kuster, Damián Sánchez-Quintana, Allard van der Wal, Vincent Christoffels; Supervision: Bjarke Jensen, Vincent M. Christoffels.

Data availability

Raw data are available from the corresponding author (b.jensen@amsterdamumc.nl) upon request.

Funding

This study was funded by an Amsterdam UMC grant 170421/2017.03.042 obtained by Antoon F. M. Moorman

Competing interest

The authors declare that there are no conflicts of interest to report.

Materials and correspondence

Dr. Bjarke Jensen, Room L2-106, Meibergdreef 15, 1105 AZ, Amsterdam, The Netherlands.
Email: b.jensen@amsterdamumc.nl, telephone: +31(0)20 5664659, twitter: @BjarkeJensen4

References

1. Jensen, B. *et al.* The hypertrabeculated (noncompacted) left ventricle is different from the ventricle of embryos and ectothermic vertebrates. *Biochim. Biophys. Acta - Mol. Cell Res.* **1863**, 1696–1706 (2016).

2. Anderson, R. H. *et al.* Key Questions Relating to Left Ventricular Noncompaction Cardiomyopathy: Is the Emperor Still Wearing Any Clothes? *Can. J. Cardiol.* **33**, 747–757 (2017).

3. Petersen, S. E. *et al.* Left Ventricular Non-Compaction - Insights From Cardiovascular Magnetic Resonance Imaging. *J. Am. Coll. Cardiol.* **46**, 101–105 (2005).

4. de la Chica, J. A. *et al.* Association Between Left Ventricular Noncompaction and Vigorous Physical Activity. *J. Am. Coll. Cardiol.* **76**, 1723–1733 (2020).

5. Oechslin, E. N., Attenhofer Jost, C. H., Rojas, J. R., Kaufmann, P. A. & Jenni, R. Long-term follow-up of 34 adults with isolated left ventricular noncompaction: A distinct cardiomyopathy with poor prognosis. *J. Am. Coll. Cardiol.* **36**, 493–500 (2000).

6. Peters, F. *et al.* Clinical outcomes in patients with isolated left ventricular noncompaction and heart failure. *J. Card. Fail.* **20**, 709–715 (2014).

7. Kovacevic-Preradovic, T. *et al.* Isolated left ventricular noncompaction as a cause for heart failure and heart transplantation: a single center experience. *Cardiology* **112**, 158–64 (2009).

8. Zemrak, F. *et al.* The relationship of left ventricular trabeculation to ventricular function and structure over a 9.5-year follow-up: The MESA study. *J. Am. Coll. Cardiol.* **64**, 1971–1980 (2014).

9. Chuang, M. L. *et al.* Correlation of trabeculae and papillary muscles with clinical and cardiac characteristics and impact on CMR measures of LV anatomy and function. *JACC Cardiovasc. Imaging* **5**, 1115–1123 (2012).

10. Tobita, K., Schroder, E. A., Tinney, J. P., Garrison, J. B. & Keller, B. B. Regional passive ventricular stress-strain relations during development of altered loads in chick embryo. *Am. J. Physiol. Circ. Physiol.* **282**, H2386–H2396 (2002).

11. Chin, T. K., Perloff, J. K., Williams, R. G., Jue, K. & Mohrmann, R. Isolated noncompaction of left ventricular myocardium. A study of eight cases. *Circulation* **82**, 507–513 (1990).

12. Towbin, J. A. & Jefferies, J. L. Cardiomyopathies Due to Left Ventricular Noncompaction, Mitochondrial and Storage Diseases, and Inborn Errors of Metabolism. *Circ. Res.* **121**, 838–854 (2017).

13. Bartram, U., Bauer, J. & Schranz, D. Primary noncompaction of the ventricular myocardium from the morphogenetic standpoint. *Pediatr. Cardiol.* **28**, 325–332 (2007).

14. Gati, S. *et al.* Reversible De Novo Left Ventricular Trabeculations in Pregnant Women. *Circulation* **130**, 475–483 (2014).

15. Hussein, A., Karimianpour, A., Collier, P. & Krasuski, R. A. Isolated Noncompaction of the Left Ventricle in Adults. *J. Am. Coll. Cardiol.* **66**, 578–585 (2015).

16. Finsterer, J., Stöllberger, C. & Towbin, J. A. Left ventricular noncompaction cardiomyopathy: cardiac, neuromuscular, and genetic factors. *Nat. Rev. Cardiol.* **14**, 224–237 (2017).

17. Choquet, C. *et al.* Deletion of Nkx2-5 in trabecular myocardium reveals the developmental origins of pathological heterogeneity associated with ventricular non-compaction cardiomyopathy. *PLOS Genet.* 1–31 (2018).

18. Wilsbacher, L. & McNally, E. M. Genetics of Cardiac Developmental Disorders: Cardiomyocyte Proliferation and Growth and Relevance to Heart Failure. *Annu. Rev. Pathol. Mech. Dis.* **11**, 395–419 (2016).

19. Faber, J. W., D'Silva, A., Christoffels, V. M. & Jensen, B. Lack of morphometric evidence for ventricular compaction in humans. *J. Cardiol.* (2021). doi:10.1016/j.jjcc.2021.03.006

20. Jenni, R., Oechslin, E., Schneider, J., Attenhofer Jost, C. & Kaufmann, P. A. Echocardiographic and pathoanatomical characteristics of isolated left ventricular non-compaction: a step towards classification as a distinct cardiomyopathy. *Heart* **86**, 666–71 (2001).

21. Jacquier, A. *et al.* Measurement of trabeculated left ventricular mass using cardiac magnetic resonance imaging in the diagnosis of left ventricular non-compaction. *Eur. Heart J.* **31**, 1098–1104 (2010).

22. Sizarov, A., Anderson, R. H., Christoffels, V. M. & Moorman, A. F. M. M. Three-dimensional and molecular analysis of the venous pole of the developing human heart. *Circulation* **122**, 798–807 (2010).

23. Sizarov, A. *et al.* Three-dimensional and molecular analysis of the arterial pole of the developing human heart. *J. Anat.* **220**, 336–349 (2012).

24. Jensen, B., van der Wal, A. C., Moorman, A. F. M. & Christoffels, V. M. Excessive trabeculations in noncompaction do not have the embryonic identity. *Int. J. Cardiol.* **227**, 325–330 (2017).

25. Moorman, A. F. M., Houweling, A. C., de Boer, P. A. J. & Christoffels, V. M. Sensitive Nonradioactive Detection of mRNA in Tissue Sections: Novel Application of the Whole-mount In Situ Hybridization Protocol. *J. Histochem. Cytochem.* **49**, 1–8 (2001).

26. Miranda-Silva, D. *et al.* Disturbed cardiac mitochondrial and cytosolic calcium handling in a metabolic risk-related rat model of heart failure with preserved ejection fraction. *Acta Physiol.* **228**, 1–17 (2020).

27. Van der Velden, J. *et al.* Increased Ca2+-sensitivity of the contractile apparatus in end-stage human heart failure results from altered phosphorylation of contractile proteins. *Cardiovasc. Res.* **57**, 37–47 (2003).

28. Rychterova, V. Principle of growth in thickness of the heart ventricular wall in the chick embryo. *Folia Morphol (Praha)* **19**, 262–272 (1971).

29. Palermo, J., Gulick, J., Colbert, M., Fewell, J. & Robbins, J. Transgenic Remodeling of the Contractile Apparatus in the Mammalian Heart. *Circ. Res.* **78**, 504–509 (1996).

30. Bayeva, M., Gheorghiade, M. & Ardehali, H. Mitochondria as a therapeutic target in heart failure. *J. Am. Coll. Cardiol.* **61**, 599–610 (2013).

31. Oechslin, E. & Jenni, R. Left ventricular non-compaction revisited: a distinct phenotype with genetic heterogeneity? *Eur. Heart J.* **32**, 1446–1456 (2011).

32. de Bakker, B. S. *et al.* An interactive three-dimensional digital atlas and quantitative database of human development. *Science* **354**, aag0053 (2016).

33. Christoffels, V. M. *et al.* Chamber formation and morphogenesis in the developing mammalian heart. *Dev. Biol.* **223**, 266–278 (2000).

34. Rhee, S. *et al.* Endothelial deletion of Ino80 disrupts coronary angiogenesis and causes congenital heart disease. *Nat. Commun.* **9**, 368 (2018).

35. Hu, Y. *et al.* Identification of cardiac hemo-vascular precursors and their requirement of sphingosine-1-phosphate receptor 1 for heart development. *Sci. Rep.* **7**, 1–13 (2017).

36. Luxán, G. *et al.* Mutations in the NOTCH pathway regulator MIB1 cause left ventricular noncompaction cardiomyopathy. *Nat. Med.* **19**, 193–201 (2013).

37. Estes, E. H., Dalton, F. M., Entman, M. L., Dixon, H. B. & Hackel, D. B. The anatomy and blood supply of the papillary muscles of the left ventricle. *Am. Heart J.* **71**, 356–362 (1966).

38. Wearn, J. T. THE EXTENT OF THE CAPILLARY BED OF THE HEART. *J. Exp. Med.* **47**, 273–290 (1928).

39. Sizarov, A. *et al.* Formation of the building plan of the human heart: Morphogenesis, growth, and differentiation Supplement. *Options* **123**, 1–5 (2011).

40. de Boer, B. A. J., van den Berg, G., de Boer, P. A. J., Moorman, A. F. M. & Ruijter, J. M. Growth of the developing mouse heart: An interactive qualitative and quantitative 3D atlas. *Dev. Biol.* **368**, 203–213 (2012).

41. Moorman, A. F. M. *et al.* Presence of functional sarcoplasmic reticulum in the developing heart and its confinement to chamber myocardium. *Dev. Biol.* **223**, 279–290 (2000).

42. Meyer, H. V *et al.* Genetic and functional insights into the fractal structure of the heart. *Nature* **584**, 589–594 (2020).

43. Seymour, R. S. & Blaylock, A. J. The Principle of Laplace and Scaling of Ventricular Wall Stress and Blood Pressure in Mammals and Birds. *Physiol. Biochem. Zool.* **73**, 389–405 (2000).

44. Weir-McCall, J. R. *et al.* Left Ventricular Noncompaction: Anatomical Phenotype or Distinct Cardiomyopathy? *J. Am. Coll. Cardiol.* **68**, 2157–2165 (2016).

45. Ivanov, A. *et al.* Prevalence and prognostic significance of left ventricular noncompaction in patients referred for cardiac magnetic resonance imaging. *Circ. Cardiovasc. Imaging* **10**, 1–10 (2017).

46. Sedmera, D., Pexieder, T., Vuillemin, M., Thompson, R. P. & Anderson, R. H. Developmental patterning of the myocardium. *Anat. Rec.* **258**, 319–337 (2000).

47. Faber, J. W., Hagoort, J., Moorman, A. F. M., Christoffels, V. M. & Jensen, B. Quantified growth of the human embryonic heart. *Biol. Open* bio.057059 (2021). doi:10.1242/bio.057059

48. Papavassiliu, T. *et al.* Effect of endocardial trabeculae on left ventricular measurements and measurement reproducibility at cardiovascular MR imaging. *Radiology* **236**, 57–64 (2005).

49. Grothoff, M. *et al.* Value of cardiovascular MR in diagnosing left ventricular non-compaction cardiomyopathy and in discriminating between other cardiomyopathies. *Eur. Radiol.* **22**, 2699–2709 (2012).

Figures

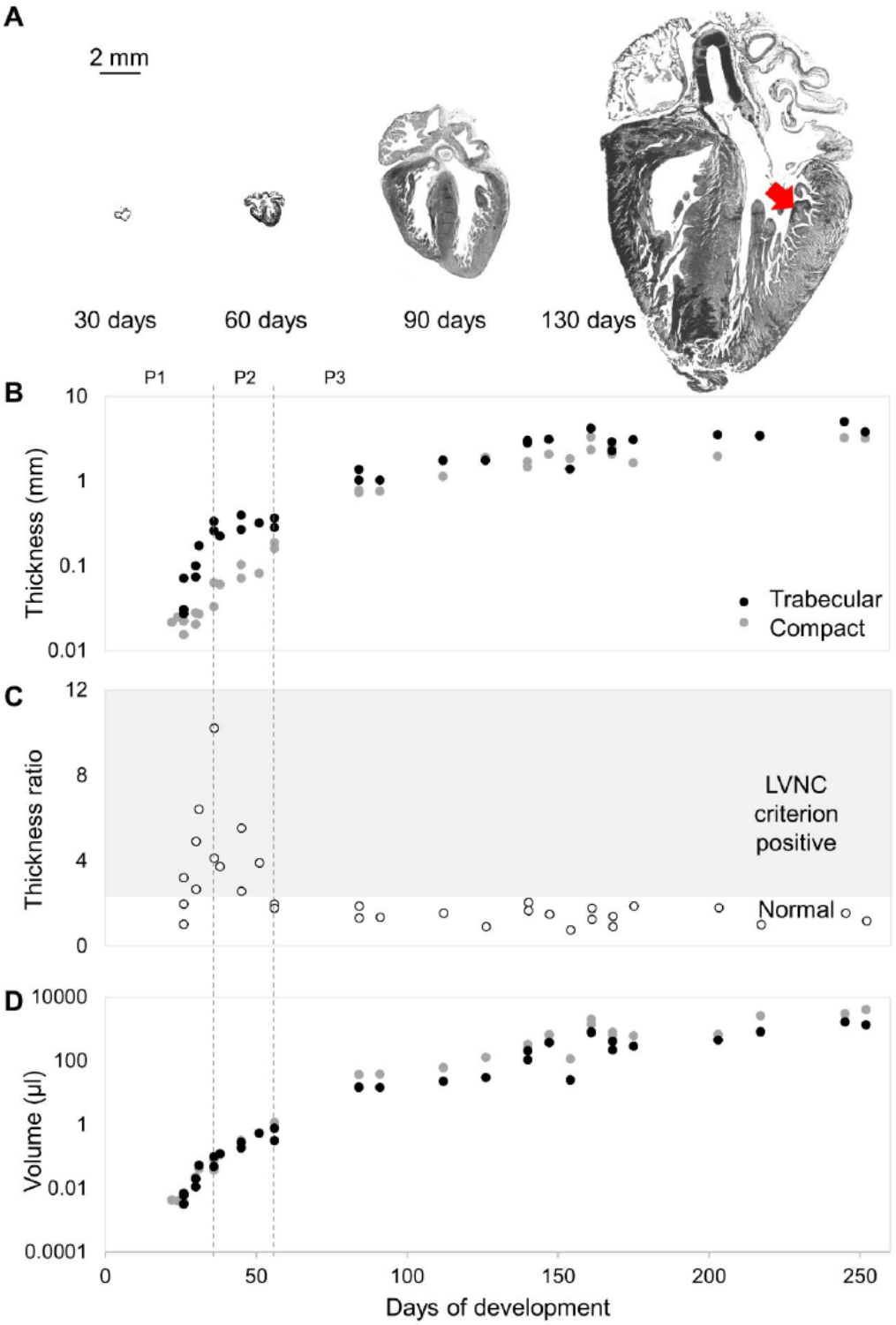

Figure 1

Growth of the human heart. Absolute size increase of human hearts between 30 and 130 days showing that the trabeculated layer in foetal stages (red arrow) is much greater than the entire embryonic heart (A). In early chamber development, between 22 and 31 gestational days (P1), the trabecular layer thickness increases more than the compact (B) which is reflected in a thickness ratio that is LVNC criterion positive (C). In late embryogenesis, between 32 and 56 gestational days (P2), the trabecular layer

thickness plateaus while the compact layer continues to thicken, this causes a drop in thickness ratio to below LVNC criterion levels. In the foetus (P3), the trabecular and compact layer thickness increase similarly which stabilises the thickness ratio. Calculated trabecular and compact volumes continuously increase in gestation, even in P2 when the thickness ratio drops dramatically (D).

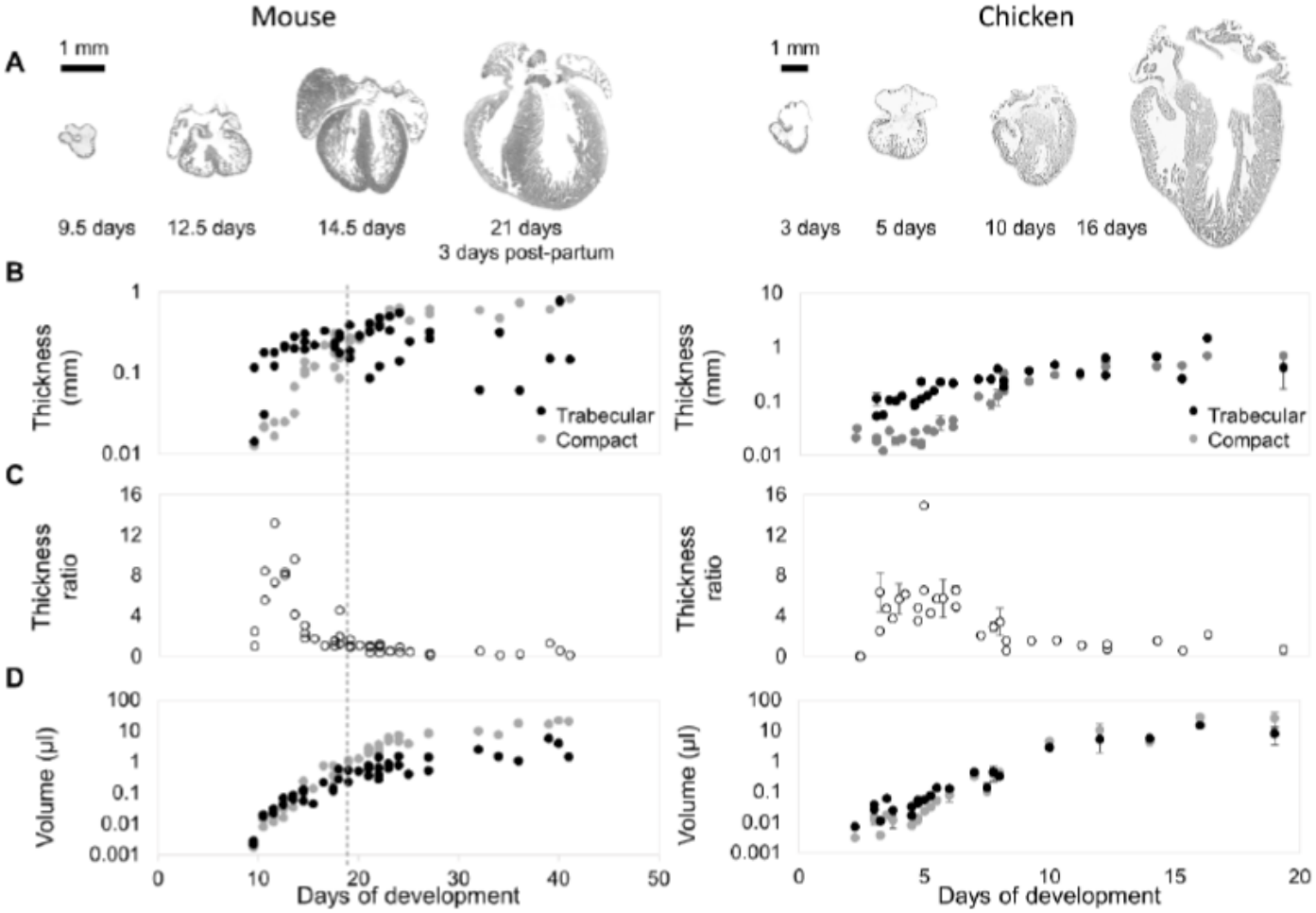

Figure 2

Growth of the mouse and chicken heart. Absolute size increase of mouse hearts between 9.5 days of gestation and 23 days postnatally, and chicken hearts between 2 and 19 days of gestation (A). In both the mouse and chicken embryo the trabecular thickness rapidly increases. Towards the end of foetal development, even continuing till after birth in mouse (dotted line), the trabecular thickness stabilises. The compact wall thickness continuously grows (B). In the embryo, the maximum peak ratio of median trabecular layer thickness over median compact layer thickness is reached while in the foetus the ratio lowers and stabilises (C). Calculated trabecular and compact volumes continuously increase (D).

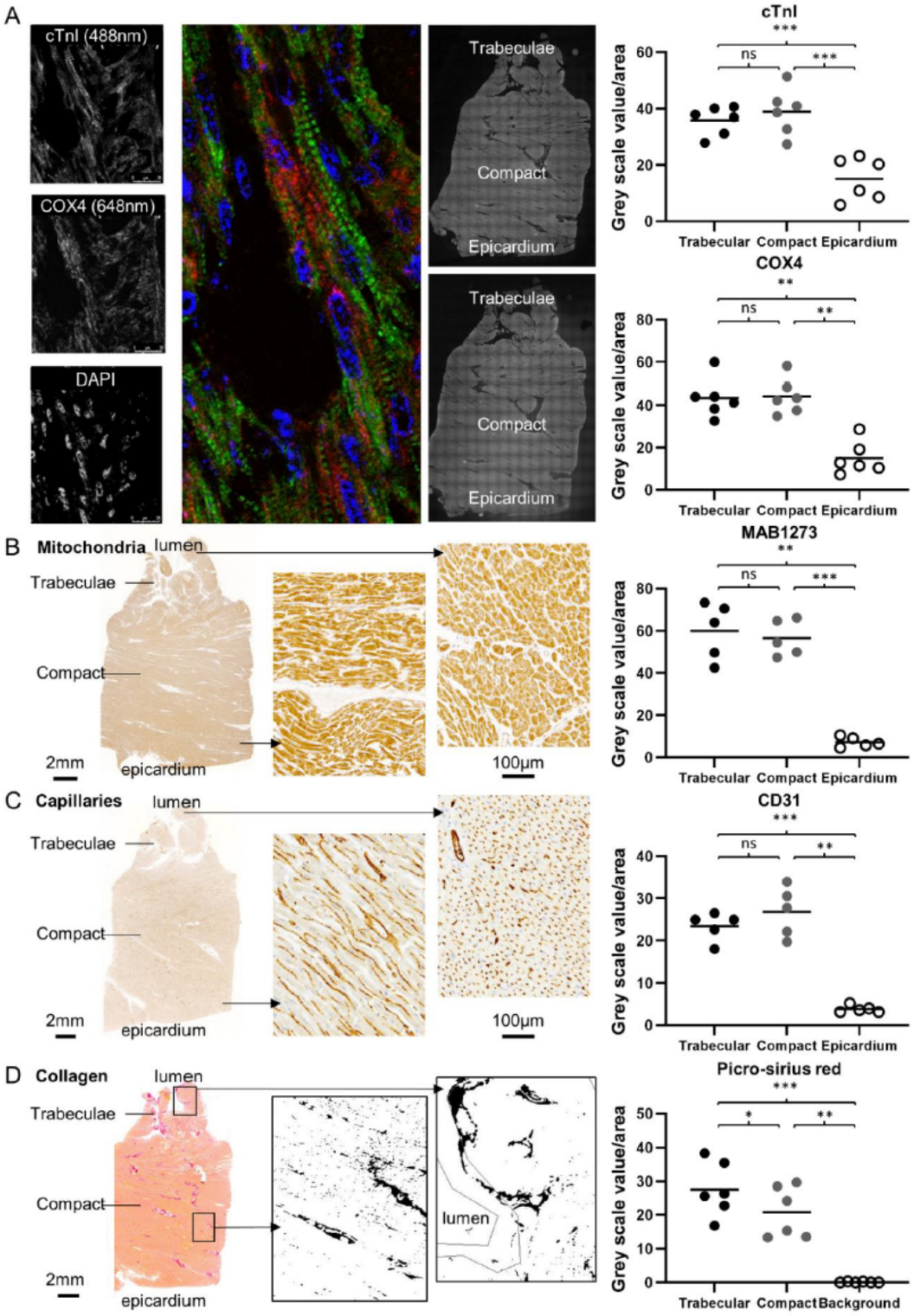

Figure 3

Trabeculated and compact tissue is similar in adult human. Staining intensity of sarcomeric protein cTnI (N=6), mitochondrial protein COX4 (N=6) (A), mitochondrial surface protein MAB1273 (N=5) (B) and endothelial marker CD31 (N=5) (C) are similar in compact and trabecular myocardium (p=0.247, p=0.857, p=0.802 and p=0.283 respectively) and greater than in epicardium. Picrosirius red stains (N=6) showed relatively more collagen in the trabecular wall compared to the compact wall (p=0.038), likely due to

insertion of chordae tendineae in the trabeculae (D). Statistical analysis: One-way ANOVA, Tukey corrected.

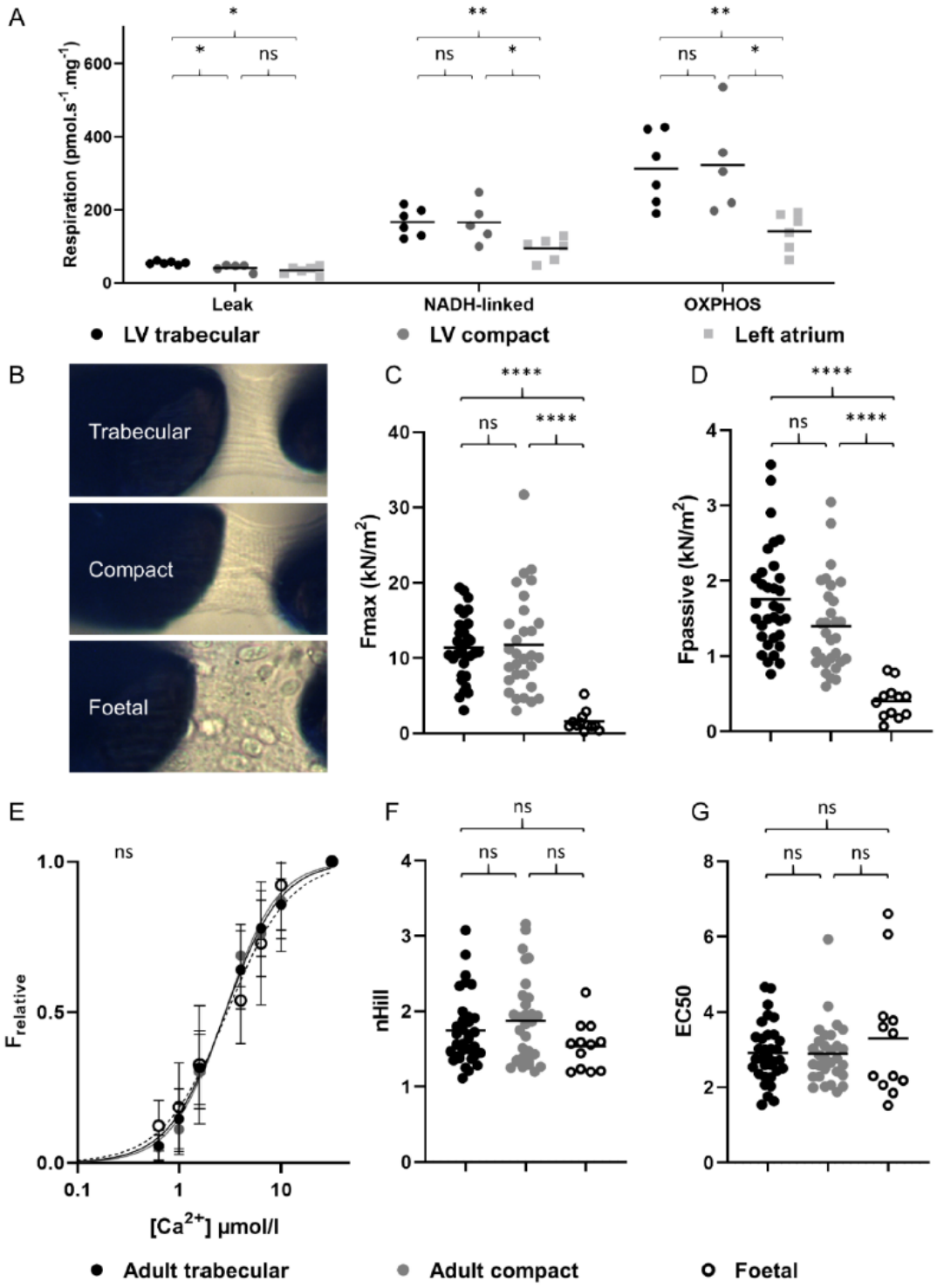

Figure 4

Functional analyses in mouse. Mitochondrial activity assay showed only a significant difference between trabecular (N=6) and compact myocardium (N=5) in leak respiration (p=0.033), for NADH-linked respiration (p=0.999) and maximal oxidative phosphorylation (OXPHOS, p=0.989) there were no

significant differences. Trabecular myocardium always had higher activity than left atrial myocardium (N=6) (p=0.027, p=0.008, p=0.008 for each treatment respectively) while compact myocardium was only more active after leak respiration (p=0.453, p=0.026, p=0.032 for each treatment respectively). Statistical analysis per condition: Mixed-effects analysis, Tukey corrected (A). Single adult trabecular and compact cardiomyocytes and a cluster of foetal cardiomyocytes as glued between the measuring needles (B). The Fmax of adult trabecular (N=31, 6 specimens) and compact cardiomyocytes (N=30, 6 specimens) is similar (p=0.959) while the foetal cardiomyocytes are significantly weaker (N=12, 2 specimens, p<0.0001) (C). The Fpas of adult trabecular and compact myocardium is similar (p=0.060) while foetal cardiomyocytes are significantly more compliant (p<0.0001) (D). Calcium dose response curves of all groups were similar (p=0.075) (E). This is reflected by similar Hill coefficients (nHill) (p=0.136) (F) and EC50 (p=0.430) (G). Statistical analysis: One-way ANOVA, Tukey corrected.

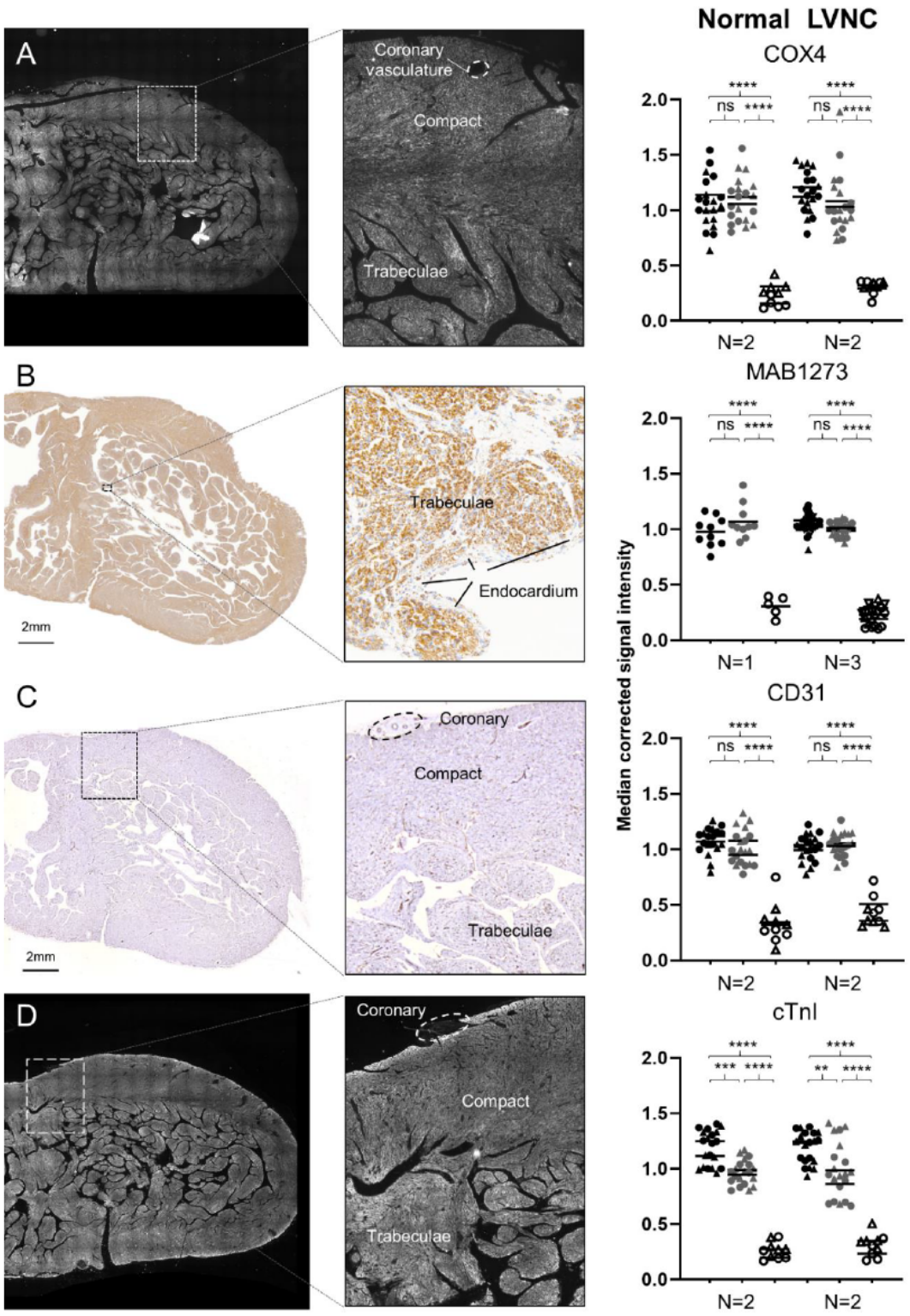

Figure 5

Trabeculated and compact tissue is similar in foetal human LVNC cases. Staining intensity of mitochondrial protein COX4 (A), mitochondrial surface protein MAB1273 (B), and endothelial protein CD31 (C) are similar in compact (black) and trabecular (grey) myocardium in normal hearts (p=1.000, p=0.224, p=0.448) and LVNC cases (p=0.574, p=0.375, p=0.990) but not in non-myocardium (open symbols) (all comparisons to non-myocardium p<0.0001). Sarcomeric protein cTnI signal intensity was

significantly higher in trabecular than in compact myocardium in normal (p=0.0003) and LVNC hearts (p=0.001) and higher than in non-myocardium (all p<0.0001) (D). Statistical analysis: One-way ANOVA, Tukey corrected.

Supplementary Files

This is a list of supplementary files associated with this preprint. Click to download.

- OnlineFigure1.png
- OnlineFigure2.png
- OnlineFigure3.png